Supporting Information

Van der Waals Graphene Kirigami Heterostructure for Strain-Controlled Thermal Transparency

Yuan Gao and Baoxing Xu *

Department of Mechanical and Aerospace Engineering, University of Virginia, Charlottesville, VA 22904, USA

* Corresponding author: bx4c@virginia.edu

Keywords: thermal transparency, van der Waals interface, graphene kirigami, heterostructure, mechanical strain

Table 1. Notation and Geometric Parameters of Kirigami Units. The length a, width b and cut length d of units are fixed as 6.89, 10.22 and 8.089 nm, respectively.

Notation	Cut Pattern (U or I)	Cut Width c (nm)	Porosity ϕ
U1	U	0.37	0.14
U2	U	0.62	0.21
U3	U	1.07	0.36
I1	I	0.98	0.26
I2	I	1.48	0.37
I3	I	1.97	0.48

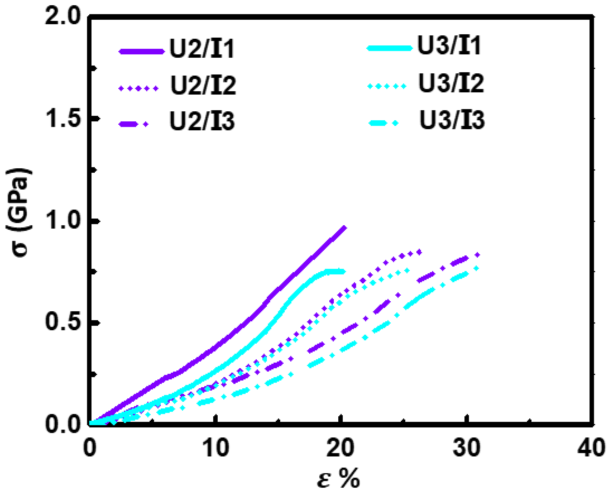

Figure S1. Nominal stress σ versus tensile strain ε of heterobilayers composed of one layer with cut pattern U (U2 and U3) and the other with cut pattern I (I1, I2 and I3).

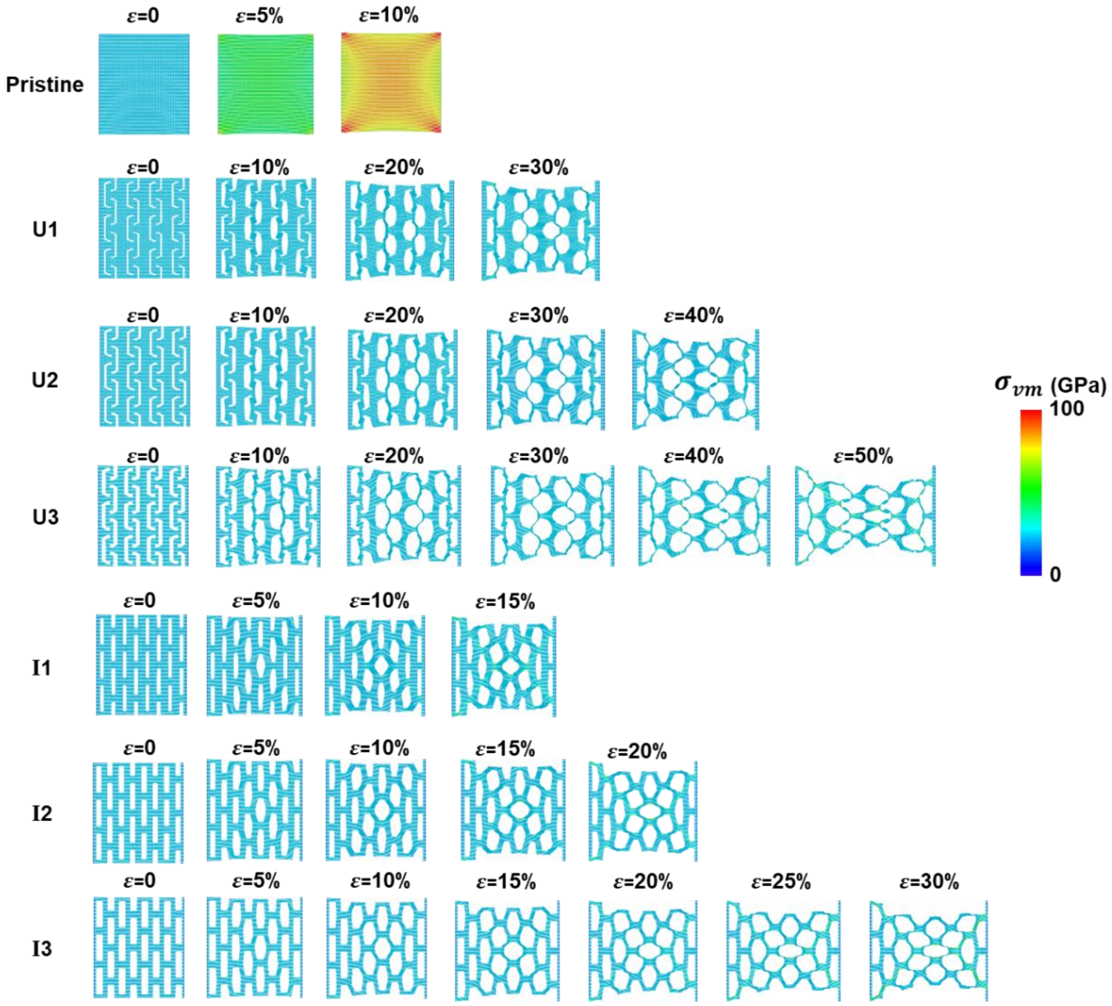

Figure S2. Von Mises stress distribution in pristine graphene and graphene kirigami with cut patterns U and I at different tensile strain ε.

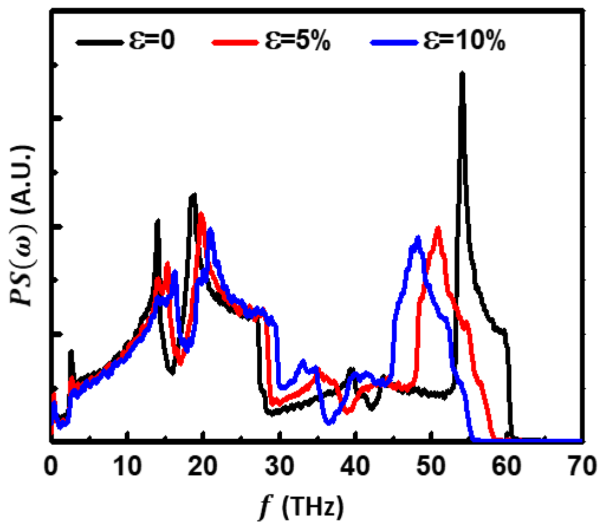

Figure S3. Vibrational spectra of carbon atoms in pristine graphene at ε=0, 5% and 15%.

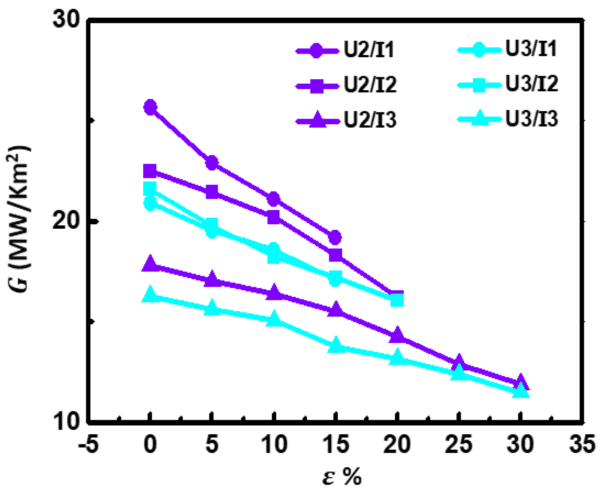

Figure S4. Thermal conductance *G* as functions of tensile strain ε in heterobilayers composed of one layer with cut pattern U (U2 and U3) and the other with cut pattern I (I1, I2 and I3).

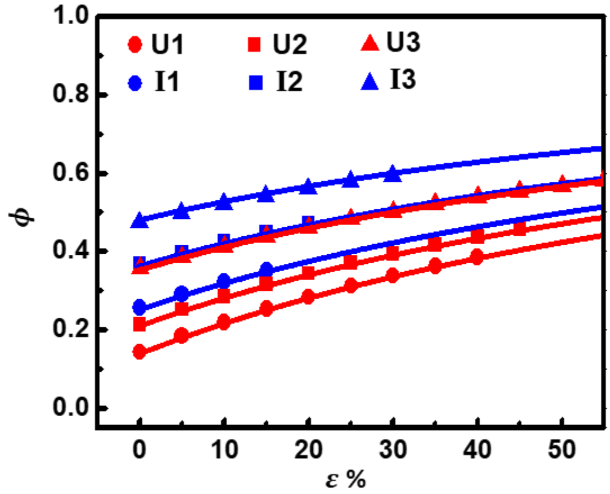

Figure S5. 2D Porosity ϕ in different graphene kirigami as functions of tensile strain. When an external tensile strain is applied to the kirigami layer, with negligible lattice definition, the increase in A is considered to fully attribute to the increase of A_{cut}. Hence the porosity at tensile strain ε can be expressed as $\phi(\varepsilon) = 1 - \frac{1-\phi(0)}{1+\varepsilon}$, where $\phi(0)$ is the porosity in the absence of tensile strain. Such expression makes good prediction for kirigami layers with different geometry (solid lines).

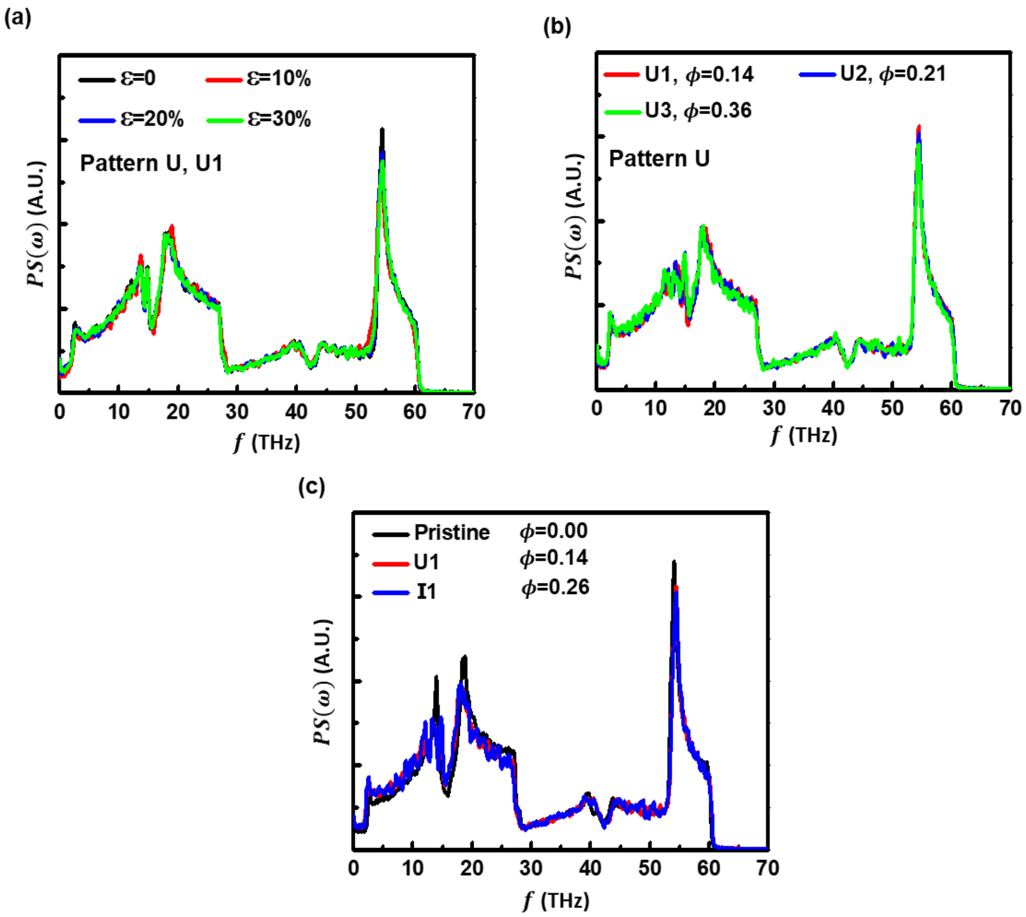

Figure S6. Vibrational spectra of graphene kirigami in heterostructures. (**a**) Effect of tensile strain. As tensile strain ε increases, the cut expands, leading to lower thermal transparency. The high frequency peak at 55 THz and the low frequency peaks at 13 and 18 THz are slightly suppressed, indicating more inconsistent motion of atoms owing to the expanded cuts in the kirigami layer and a lower thermal conductance. Same conclusion can be drawn when increasing the size of cuts, as shown by (**b**). The same statement still holds true when making comparison between different basic patterns, demonstrated by (**c**).

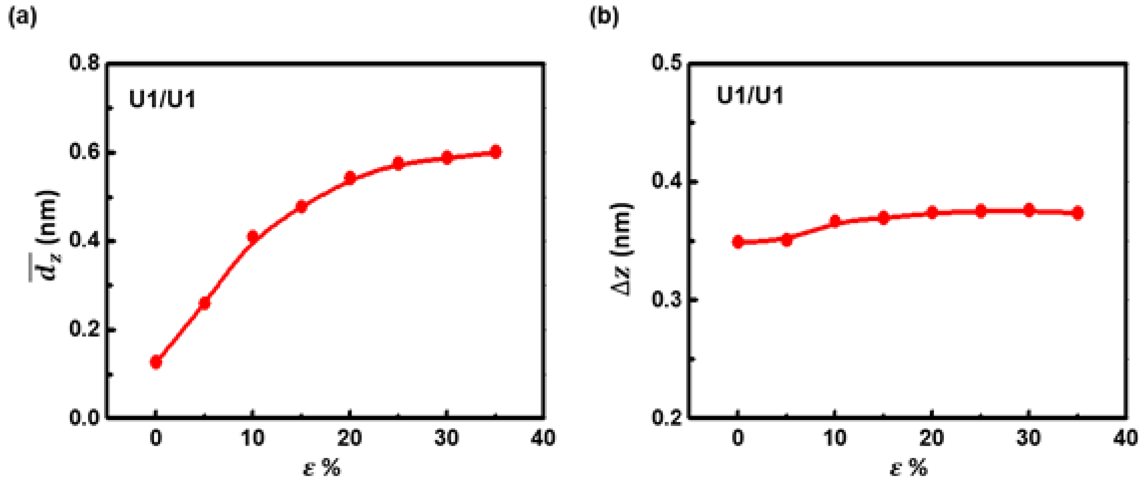

Figure S7. Out-of-plane displacement in graphene kirigami at tensile strain. (**a**) Averaged magnitude of out-of-plane displacement as a function of tensile strain. (**b**) Distance between the centers of mass of two layers as a function of tensile strain. The increase in the distance between the centers of mass is limited by the mechanical flexibility and conformal attachment between layers.

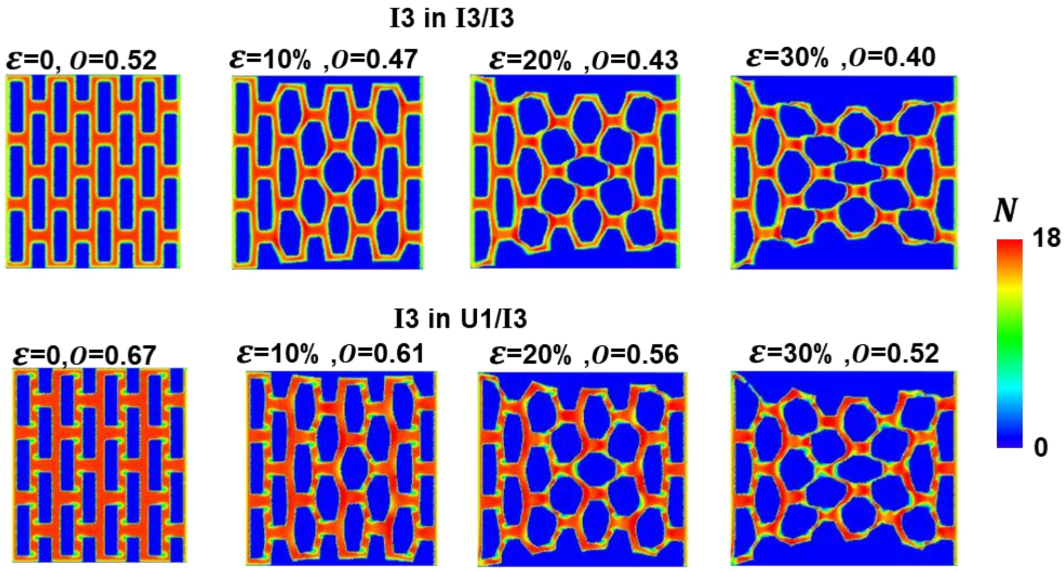

Figure S8. Distribution of interaction N in kirigami layer I3 in homobilayers I3/I3 and heterobilayers U1/I3.

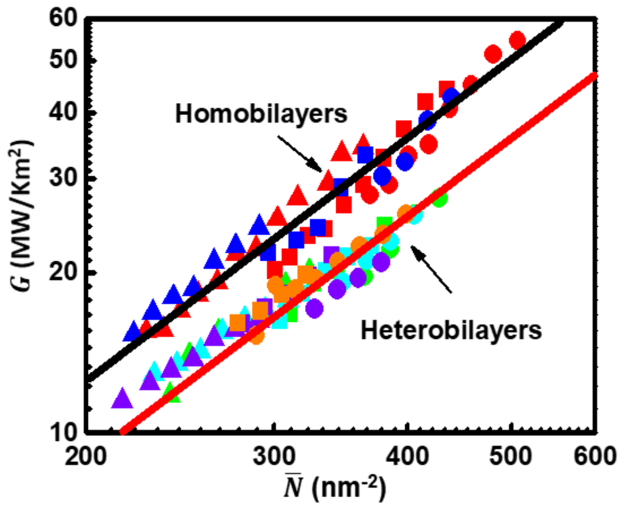

Figure S9. Thermal conductance G as functions of density of interactions $\bar{N}$. While sharing the same slope with the linear function of homobilayers, the relationship between the thermal conductance and density of interactions is down shifted, which indicate the quality of each interaction is reduced in heterobilayers. Homobilayers: U1/U1 (red circles), U2/U2 (red squares), U3/U3 (red triangles), I1/I1 (blue circles), I2/I2 (blue squares), I3/I3 (blue triangles); Heterobilayers: U1/I1 (green circles), U1/I2 (green squares), U1/I3 (green triangles), U2/I1 (cyan circles), U2/I2 (cyan squares), U2/I3 (cyan triangles), U3/I1 (purple circles), U3/I2 (purple squares), U3/I3 (purple triangles), U1/U3 (orange circles) and I1/I3 (orange squares).

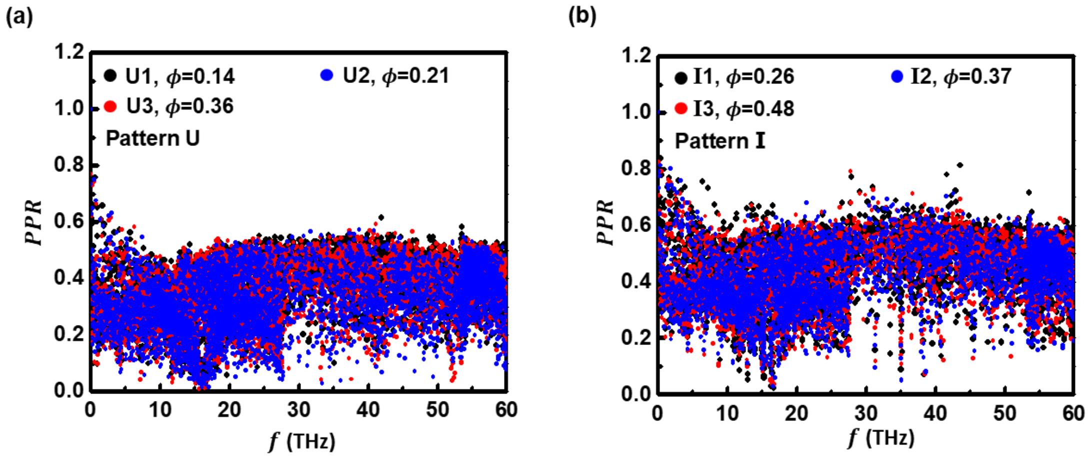

Figure S10. Phonon participation ratio (PPR) of eigenmodes at different frequency f in kirigami layers. As the sizes of cuts increase, the phonon participation ratio slightly reduces in pattern U (**a**) and pattern I (**b**).

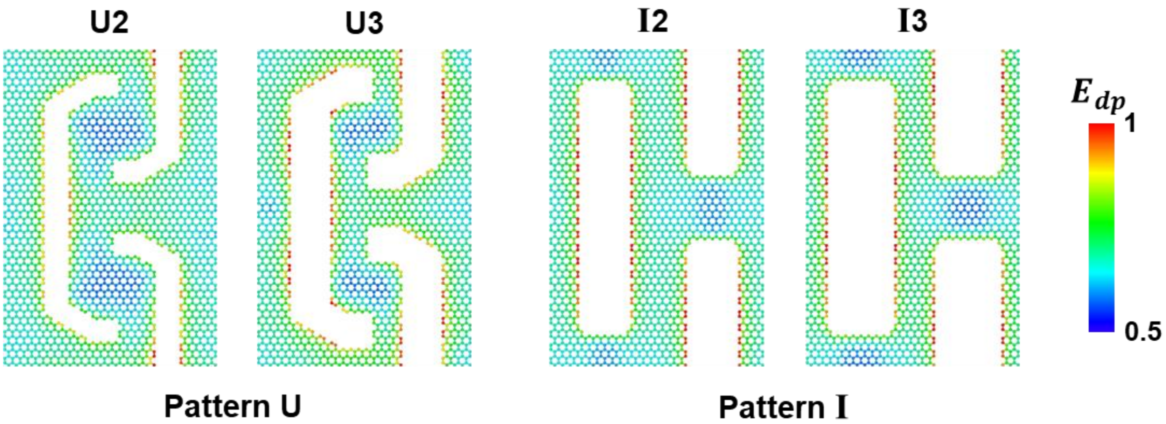

Figure S11. Distribution of normalized energy of delocalized phonon ($PPR > 0.4$) in the unit cell of kirigami layers with cut patterns U2, U3, I2 and I3.

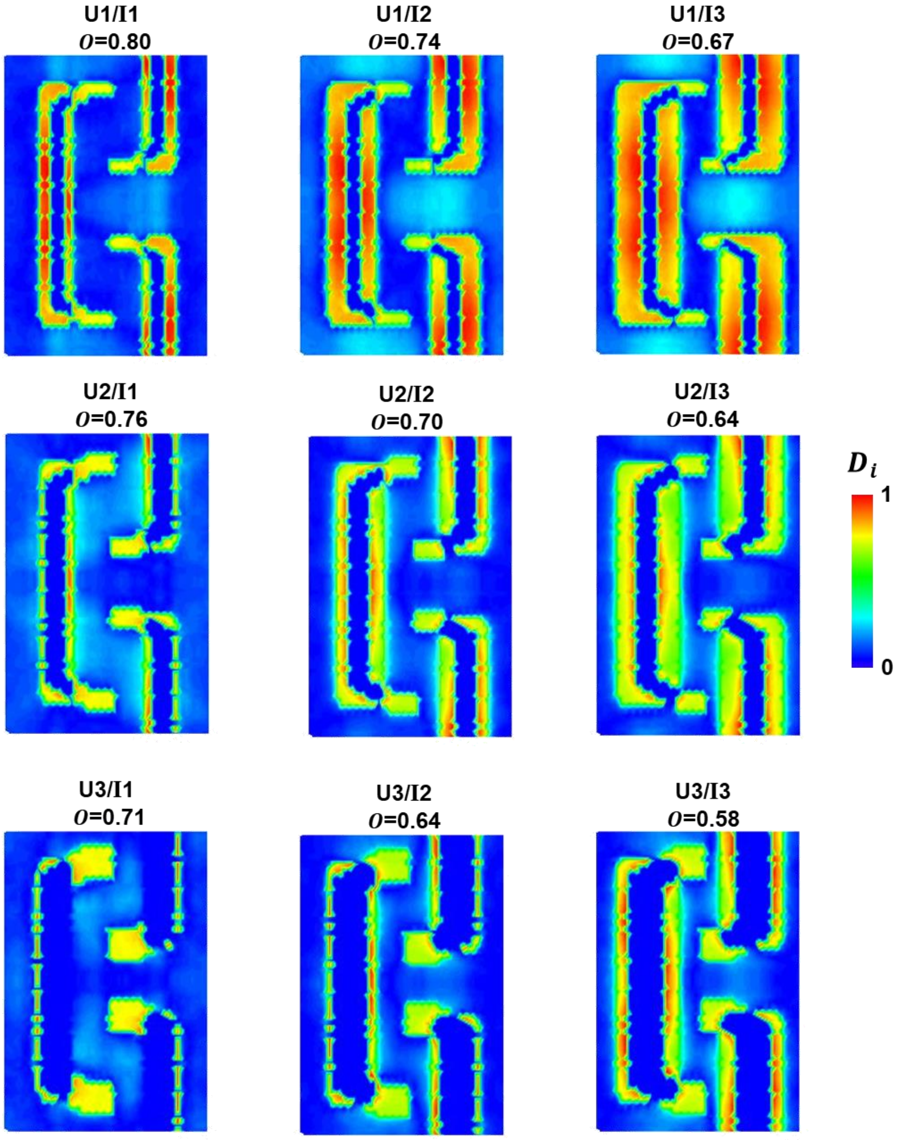

Figure S12. Difference in the distribution of delocalized phonon energy in heterobilayers composed of kirigami layers with different basic patterns and porosities.

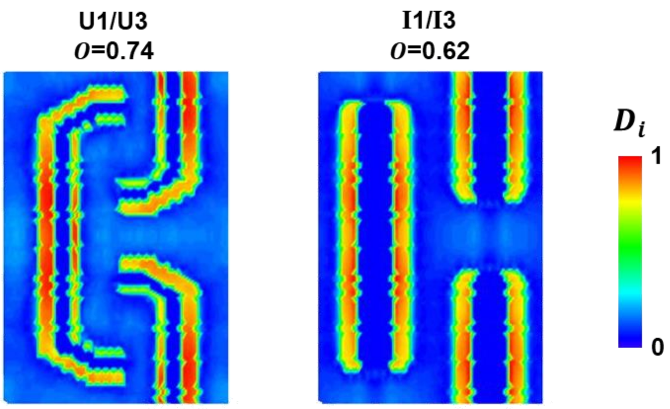

Figure S13. Difference in the distribution of delocalized phonon energy in heterobilayers composed of layers with the same basic pattern but different porosities.

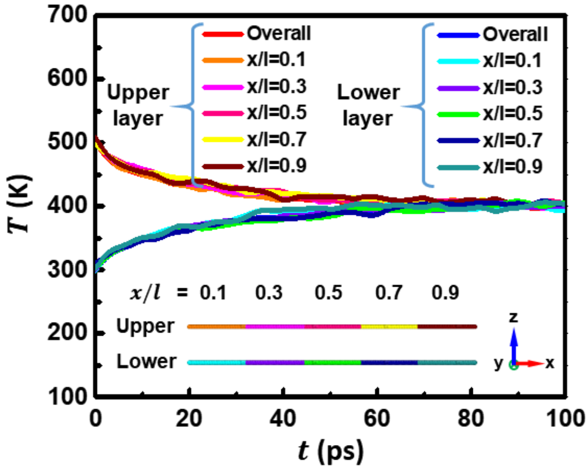

Figure S14. Overall and local temperature at different relative x-coordinates in upper and lower kirigami layers in homobilayer U1/U1 as functions of simulation time. The inset demonstrates the slabs in the model for calculating local temperature values.